

Supporting Information

for

Ammonium Vanadium Oxide [(NH₄)₂V₄O₉] Sheets for High Capacity Electrodes in Aqueous Zinc Ion Batteries

Yifu Zhang, Hanmei Jiang, Lei Xu, Zhanming Gao, Changgong Meng*

School of Chemical Engineering, Dalian University of Technology, Dalian 116024, PR China

*E-mail address: cgmeng@dlut.edu.cn

Experimental section

Synthesis of $(\text{NH}_4)_2\text{V}_4\text{O}_9$ sheets

All chemicals purchased from Sinopharm Chemical Reagent Co., Ltd were with analytical grade and used without any further purification. In a typical procedure, 0.585 g of NH_4VO_3 , 0.4725 g of $\text{H}_2\text{C}_2\text{O}_4 \cdot 2\text{H}_2\text{O}$ and 35 mL distilled water were mixed and magnetic stirred for 30 min at the room temperature. The above solution was transferred into a 50 mL Teflon-lined stainless steel autoclave and kept at 180 °C for 48 h. After the reaction, the products were filtered off, washed with distilled H_2O and absolute ethanol several times to remove any possible residues, and dried in vacuum at 75 °C over night to obtain $(\text{NH}_4)_2\text{V}_4\text{O}_9$ sheets.

Materials characterization

The phase and composition of the products were identified by X-ray powder diffraction (XRD, Panalytical X'Pert powder diffractometer at 40 kV and 40 mA with Ni-filtered $\text{Cu K}\alpha$ radiation). The chemical composition of as-obtained samples was revealed by use of an energy-dispersive X-ray spectrometer (EDS) and EDS mapping attached to a scanning electron microscope (SEM, QUANTA450). X-ray photoelectron spectroscopy (XPS) was used to investigate the composition of the products and confirm the oxidation state of vanadium performed on ESCALAB250Xi, Thermo Fisher Scientific. The Raman spectra were obtained using a Thermo Scientific spectrometer, with a 532 nm excitation line. Fourier transform infrared spectroscopy (FTIR) pattern of the solid samples was measured using KBr pellet technique (About 1 wt. % of the samples and 99 wt. % of KBr were mixed homogeneously, and then the mixture was pressed to a pellet) and recorded on a Nicolet 6700 spectrometer from 4000 to 400 cm^{-1} with a resolution of 4 cm^{-1} . The morphology and dimensions of the products were observed by field emission scanning electron microscopy (FE-SEM, NOVA NanoSEM 450, FEI) and transmission electron microscopy (TEM, FEITecnai F30, FEI). The high-resolution transmission electron microscopy (HRTEM) and selected area electron diffraction (SAED) were also carried out on FEITecnai F30. The samples were dispersed in absolute ethanol with ultrasonication before TEM characterization.

For the ex situ XRD, Raman and XPS characterizations, the cycled electrodes were washed with deionized water and dried naturally in air. But as for the ex situ TEM investigations, the cycled electrodes could easily peel off from the titanium foil and then ultrasound with alcohol.

Electrochemical characterization

Electrochemical tests of the $(\text{NH}_4)_2\text{V}_4\text{O}_9$ were performed with CR2032 coin-type cells. The working electrode was fabricated by mixing the active material, a conductive agent (Super-P, Sigma-Aldrich), and PVDF (Sigma-Aldrich), in a weight ratio of 7 : 2 : 1. Next, the mixture was coated on Ti sheet. The total mass of the electrode materials was around 2 mg, measured by an ultramicro analytical balance (Mettler Toledo XP2U, 0.1 mg resolution). After drying in air at 90 °C for 12 h, the electrodes were assembled in coin type cells (CR2032) and zinc foil and glass fiber (Whatman GF/A) were employed as the anode and separator, respectively. A 3 M $\text{Zn}(\text{CF}_3\text{SO}_3)_2$ aqueous solution was used as the electrolyte. Cyclic voltammetry (0.3–1.3 V) and EIS were performed on a CHI 660D electrochemical workstation. The charge/discharge tests were performed using a Wuhan LAND battery tester at different current rates.

Figure S1

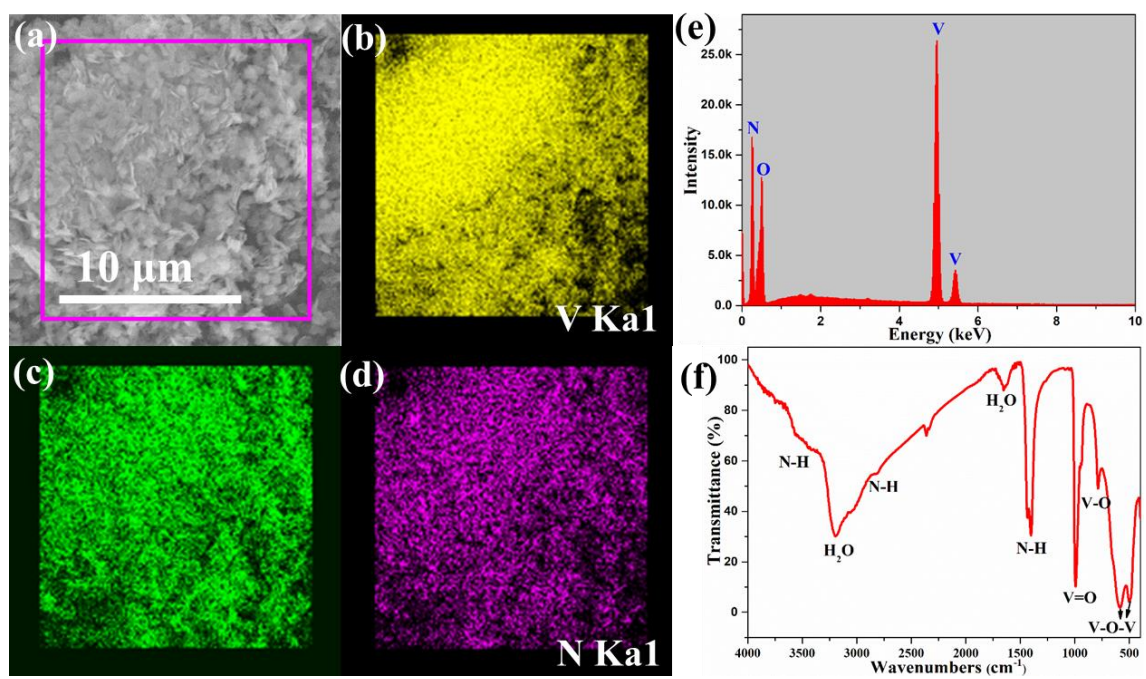


Figure S1. The composition of $(\text{NH}_4)_2\text{V}_4\text{O}_9$ sheets: (a-d) Elemental mapping images; (e) EDS spectrum; (f) FTIR spectrum.

Figure S2

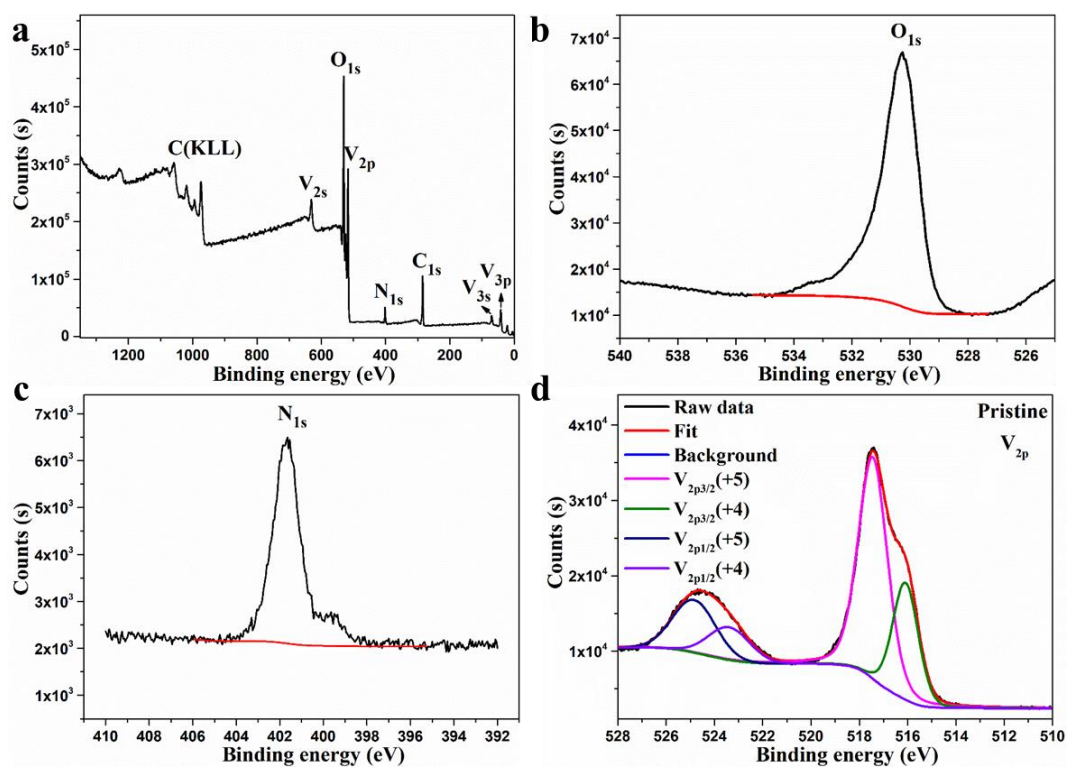


Figure S2. XPS spectra of $(\text{NH}_4)_2\text{V}_4\text{O}_9$ sheets: (a) full spectrum; (b) core-level spectrum of O_{1s} ; (c) core-level spectrum of N_{1s} ; (d) core-level spectrum of V_{2p} .

Figure S3

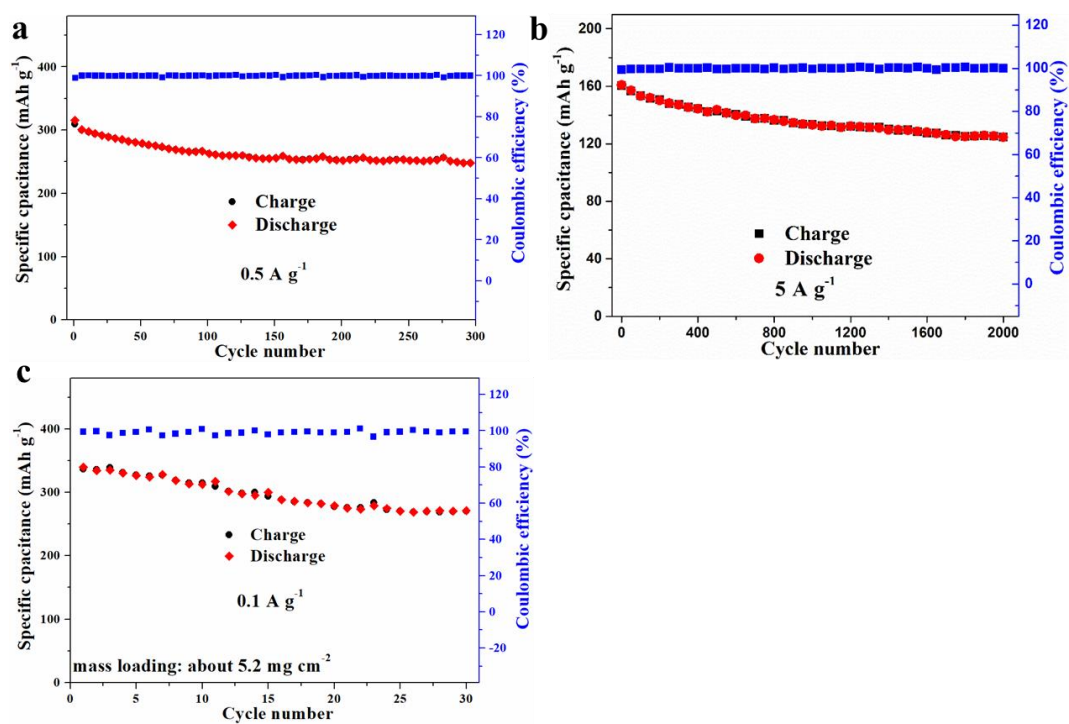


Figure S3. Cycling performance at 0.5 A g^{-1} (a) and 5 A g^{-1} (b) of Zn// $(\text{NH}_4)_2\text{V}_4\text{O}_9$ battery. (c) Cycling performance with high mass loading at 0.1 A g^{-1} of Zn// $(\text{NH}_4)_2\text{V}_4\text{O}_9$ battery.

Figure S4

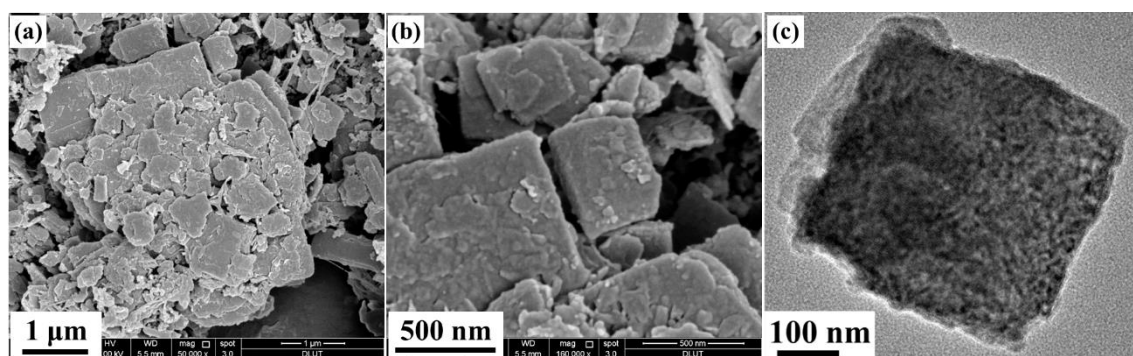


Figure S4. FE-SEM (a, b) and TEM (c) images of $(\text{NH}_4)_2\text{V}_4\text{O}_9$ in $\text{Zn}/(\text{NH}_4)_2\text{V}_4\text{O}_9$ battery after cycles.

Table S1

Table S1. Comparison of previous related ARZIB cathode materials with this work.

Cathode Materials	Electrochemical Performance (Capacity retention)	Ref.
(NH₄)₂V₄O₉	328 mA h g⁻¹ at 0.1 A·g⁻¹ after 100 cycles	This work
	262 mA h g⁻¹ at 0.2 A·g⁻¹ after 100 cycles	
	259 mA h g⁻¹ at 0.5 A·g⁻¹ after 300 cycles	
	125 mA h g⁻¹ at 5 A g⁻¹ after 2000 cycles	
LiV ₃ O ₈	172 mA h g ⁻¹ at 0.133 A g ⁻¹ after 65 cycles	1
Fe ₅ V ₁₅ O ₃₉ (OH) ₉ ·9H ₂ O	About 100 mA h g ⁻¹ at 5 A g ⁻¹ after 300 cycles	2
V ₂ O ₅	110 mA h g ⁻¹ at 2 A g ⁻¹ after 2000 cycles	3
VO _{1.52} (OH) _{0.77}	105 mA h g ⁻¹ at 0.015 A g ⁻¹ after 50 cycles	4
H ₂ V ₃ O ₈	136.1 mA h g ⁻¹ at 5 A g ⁻¹ after 1000 cycles	5
V ₂ O ₅ ·nH ₂ O	About 220 mA h g ⁻¹ at 6 A g ⁻¹ after 900 cycles	6
K ₂ V ₈ O ₂₁	128.3 mA h g ⁻¹ at 6 A g ⁻¹ after 300 cycles	7
Ag _{0.4} V ₂ O ₅	144 mA h g ⁻¹ at 20 A g ⁻¹ after 4000 cycles	8
VS ₂	110.9 mA h g ⁻¹ at 0.5 A g ⁻¹ after 200 cycles	9
α-Zn ₂ V ₂ O ₇	138 mA h g ⁻¹ at 4 A g ⁻¹ after 1000 cycles	10
Zn ₃ V ₂ O ₇ (OH) ₂ ·2H ₂ O	101mA h g ⁻¹ at 0.2 A g ⁻¹ after 300 cycles	11
ZnMn ₂ O ₄	106.5 mA h g ⁻¹ at 0.1 A g ⁻¹ after 300 cycles	12
Na _{1.1} V ₃ O _{7.9} @rGO	171 mA h g ⁻¹ at 0.3 A g ⁻¹ after 100 cycles	13
MnO ₂	135 mA h g ⁻¹ at 2 A g ⁻¹ after 2000 cycles	14
β-MnO ₂	135 mA h g ⁻¹ at 0.2 A g ⁻¹ after 200 cycles	15
α-Mn ₂ O ₃	82.2 mA h g ⁻¹ at 2 A g ⁻¹ after 1000 cycles	16
Mn ₃ O ₄	106.1 mA h g ⁻¹ at 0.5 A g ⁻¹ after 300 cycles	17
ZnHCF@MnO ₂	About 80 mA h g ⁻¹ at 0.5 A g ⁻¹ after 1000 cycles	18
Na ₃ V ₂ (PO ₄) ₂ F ₃	63.8 mA h g ⁻¹ at 6 A g ⁻¹ after 600 cycles	19

Table S2

Table S2. Comparison of the electrochemical performance of $(\text{NH}_4)_2\text{V}_4\text{O}_9$ with the state-of-the-art reported cathode materials.

Cathode Materials	Electrochemical Performance	Ref.
$(\text{NH}_4)_2\text{V}_4\text{O}_9$	356, 327, 299, 261 and 232 mA h g⁻¹ at 0.1, 0.2, 0.3, 0.4 and 0.5 A g⁻¹	This work
$(\text{NH}_4)_2\text{V}_3\text{O}_8$	~160 mAh g ⁻¹ at 0.1 A g ⁻¹	20
$\text{NH}_4\text{V}_4\text{O}_{10}$	361.6 mAh g ⁻¹ at 1 A g ⁻¹ 380.3 mAh g ⁻¹ at 0.1 A g ⁻¹	20
$\text{NH}_4\text{V}_3\text{O}_8$	~80 mAh g ⁻¹ at 0.1 A g ⁻¹	20
$(\text{NH}_4)_2\text{V}_{10}\text{O}_{25} \cdot 8\text{H}_2\text{O}$	228.8 mAh g ⁻¹ at 0.1 A g ⁻¹	21
$\text{NH}_4\text{V}_4\text{O}_{10}$ nanobelt	147 mAh g ⁻¹ at 0.05 A g ⁻¹	22
$\text{Zn}_{0.25}\text{V}_2\text{O}_5 \cdot n\text{H}_2\text{O}$	300, 260 and 223 mAh g ⁻¹ at C/6, 1 C, and 15 C, respectively. (1C=300 mA g ⁻¹)	23
$\text{Mg}_{0.34}\text{V}_2\text{O}_5 \cdot n\text{H}_2\text{O}$	353, 330, 291, 264 and 81 mAh g ⁻¹ at 0.05, 0.1, 0.5, 1 and 5 A g ⁻¹ , respectively	24
$\text{Ca}_{0.25}\text{V}_2\text{O}_5 \cdot n\text{H}_2\text{O}$	340, and 289 mAh g ⁻¹ at 0.2 C and 1C, respectively. (1C=250 mA g ⁻¹)	25
LiV_3O_8	256, 311, 172, 148, and 47 mAh g ⁻¹ at 0.016, 0.066, 0.133, 0.266 and 1.066 A g ⁻¹ , respectively.	1
$\text{Na}_{1.1}\text{V}_3\text{O}_{7.9}$ nanoribbons/graphene	191 mAh g ⁻¹ at 0.05 A g ⁻¹	13
$\text{Na}_{0.33}\text{V}_2\text{O}_5$ nanowire	367.1, 253.7, 173.4, 137.5 and 96.4 mAh g ⁻¹ at 0.1, 0.2, 0.5, 1, and 2 A g ⁻¹ , respectively.	26
$\text{Na}_5\text{V}_{12}\text{O}_{32}$ ($\text{Na}_{1.25}\text{V}_3\text{O}_8$)	281 mAh g ⁻¹ at 0.5 A g ⁻¹	27
$\text{HNaV}_6\text{O}_{16} \cdot 4\text{H}_2\text{O}$ ($\text{H}_{0.5}\text{Na}_{0.5}\text{V}_3\text{O}_8 \cdot 2\text{H}_2\text{O}$)	304 mAh g ⁻¹ at 0.5 A g ⁻¹	27
β - $\text{Na}_{0.33}\text{V}_2\text{O}_5$ -type tunneled structure $\text{Na}_{0.76}\text{V}_6\text{O}_{15}$ ($\text{Na}_{0.253}\text{V}_2\text{O}_5$)	135 mAh g ⁻¹ at 0.5 A g ⁻¹	27
$\text{Na}_2\text{V}_6\text{O}_{16} \cdot 1.63\text{H}_2\text{O}$ nanowire	352, 261, and 219 mAh g ⁻¹ at 0.05, 0.5 and 1 A g ⁻¹ , respectively	28
$\text{Zn}_3\text{V}_2\text{O}_7(\text{OH})_2 \cdot 2\text{H}_2\text{O}$	200, 122, 84 and 54 mAh g ⁻¹ at 0.05, 0.5, 1 and 3 A g ⁻¹ , respectively	11
$\text{Zn}_2(\text{OH})\text{VO}_4$	204, 160 and 101 mAh g ⁻¹ at 0.5 C, 10 C and 50 C, respectively. (1 C= 200 mA g ⁻¹)	29
$\text{Fe}_5\text{V}_{15}\text{O}_{39}(\text{OH})_9 \cdot 9\text{H}_2\text{O}$	385 mAh g ⁻¹ at 0.1A g ⁻¹	2
α - $\text{Zn}_2\text{V}_2\text{O}_7$	248, 231, 223, 218, 213, 209, 205, 190, and 170 mAh g ⁻¹ at 50, 100, 200, 300, 500, 700, 900, 1100, 2200, and 4400 mA g ⁻¹ , respectively.	10
$\text{VO}_2(\text{B})$ nanofibers	357 mAh g ⁻¹ at 0.1 A g ⁻¹	30
$\text{VO}_2(\text{B})/\text{rGO}$	365 mAh g ⁻¹ at 0.05 A g ⁻¹	31

VO ₂ (B)	338 mAh g ⁻¹ at 0.05 A g ⁻¹	31
VO ₂ (B) nanobelts	274 mAh g ⁻¹ at 0.1 A g ⁻¹	32
RGO/VO ₂ composite	276 mAh g ⁻¹ at 0.1 A g ⁻¹	33
H ₂ V ₃ O ₈ nanowire	423.8 mAh g ⁻¹ at 0.1 A g ⁻¹	5
V ₂ O ₅	215 mAh g ⁻¹ at 0.1 A g ⁻¹	3
H ₂ V ₃ O ₈ nanowire/Graphene	394 mAh g ⁻¹ at 0.1 A g ⁻¹	34
V ₁₀ O ₂₄ ·12H ₂ O	164.5 mAh g ⁻¹ at 0.2 A g ⁻¹ after 2 cycles	35
V ₂ O ₅ ·nH ₂ O/graphene	381 mAh g ⁻¹ at 0.3 A g ⁻¹	6
V ₂ O ₅	470 mAh g ⁻¹ at 0.2 A g ⁻¹	36
V ₂ O ₅ nanofibers	319 mAh g ⁻¹ at 0.02 A g ⁻¹	37
V ₆ O ₁₃ ·nH ₂ O	395 mAh g ⁻¹ at 0.1 A g ⁻¹	38
V ₂ O ₅ nanospheres	188.7 mAh g ⁻¹ at 0.5 A g ⁻¹	39
V ₂ O ₅ nanopaper	375 mAh g ⁻¹ at 0.5 A g ⁻¹	40
V ₂ O ₅ hollow spheres	280 mAh g ⁻¹ at 0.2 A g ⁻¹	41
VS ₂	190.3, 136.8 and 121.5 mAh g ⁻¹ at 0.05, 0.5 and 1 A g ⁻¹ , respectively	42
VS ₄ @rGO	~250 mAh g ⁻¹ at 0.2 A g ⁻¹	43

Figure S5

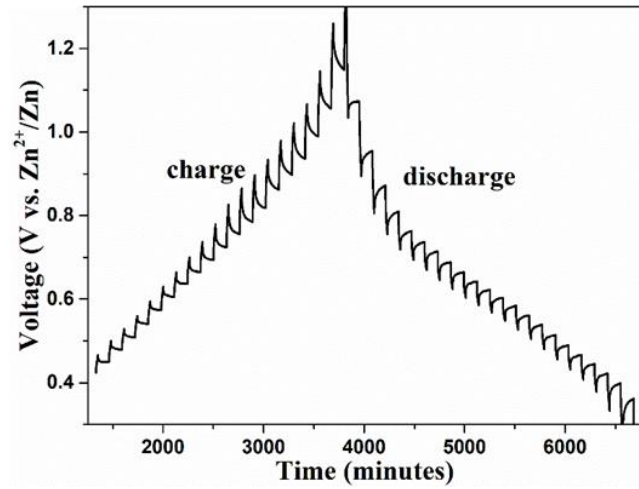


Figure S5. GITT curves: the voltage vs. the discharge/charge time.

Before the GITT measurement, the assembled cell was first discharged/charged at 100 mA g^{-1} for 6 cycles to obtain a stable state. Subsequently, the cell was discharged or charged at 100 mA g^{-1} for 20 min, and then relaxed for 120 min to make the voltage reach the equilibrium. The procedure was repeatedly applied to the cell during the entire charge/discharge process. The Zn^{2+} diffusion coefficient can be calculated based on the following equation^{36,44}:

$$D_{\text{Zn}^{2+}} = \frac{4}{\pi\tau} \left(\frac{m_B V_M}{M_B S} \right)^2 \left(\frac{\Delta E_S}{\Delta E_\tau} \right)^2$$

where τ is the duration time of the current pulse, m_B is the mass of the active material, M_B is the molecular weight (g/mol) and V_M is its molar volume (cm^3/mol), S is the total contacting area of electrode with electrolyte, ΔE_S and ΔE_τ are the change in the steady state voltage and overall cell voltage after the application of a current pulse in a single step GITT experiment, respectively.

Figure S6

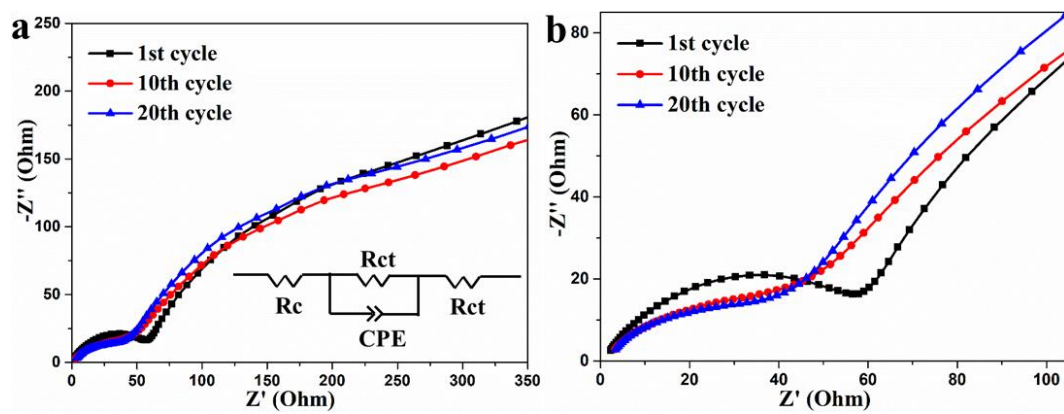


Figure S6. Nyquist plots after different discharge/charge processes of Zn// $(\text{NH}_4)_2\text{V}_4\text{O}_9$ battery.

Figure S7

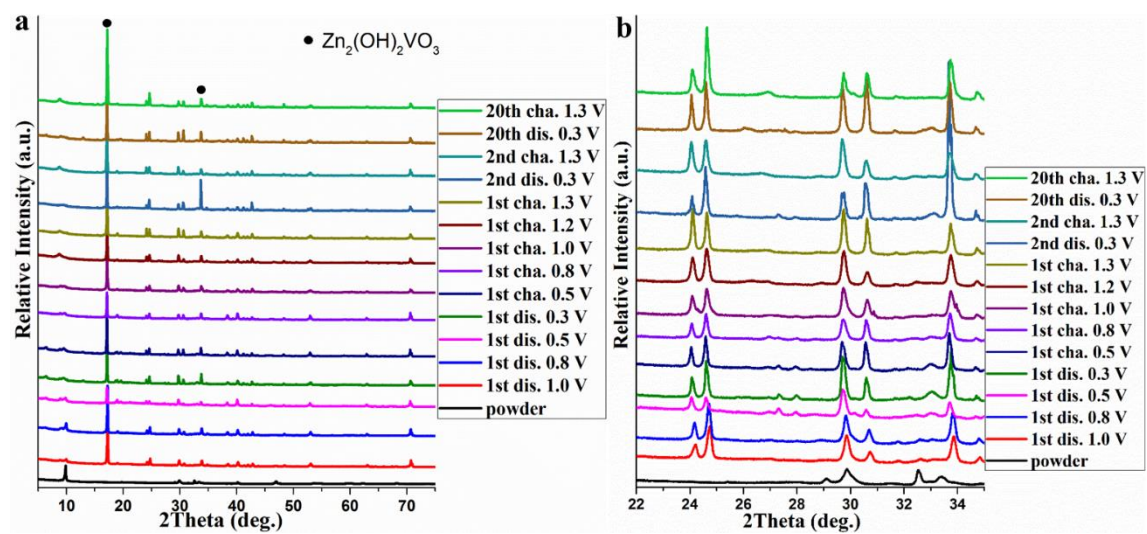


Figure S7. *Ex situ* XRD patterns of the material at different discharge/charge states in Zn// $(\text{NH}_4)_2\text{V}_4\text{O}_9$ battery.

Figure S8

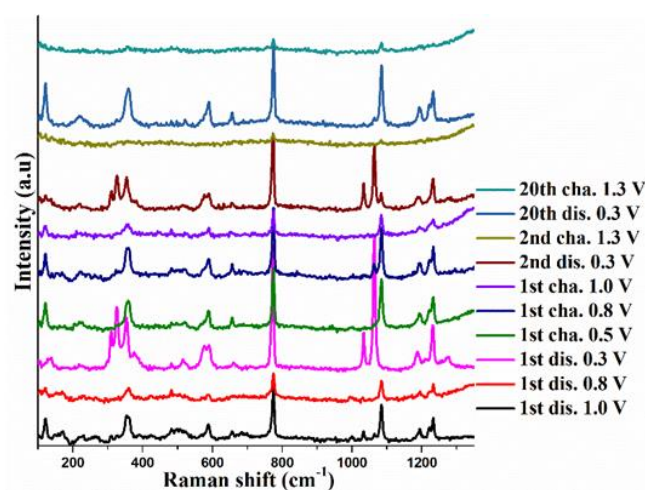


Figure S8. *Ex situ* Raman spectra of the cathode materials of different discharge/charge states in

Zn// $(\text{NH}_4)_2\text{V}_4\text{O}_9$ battery.

Figure S9

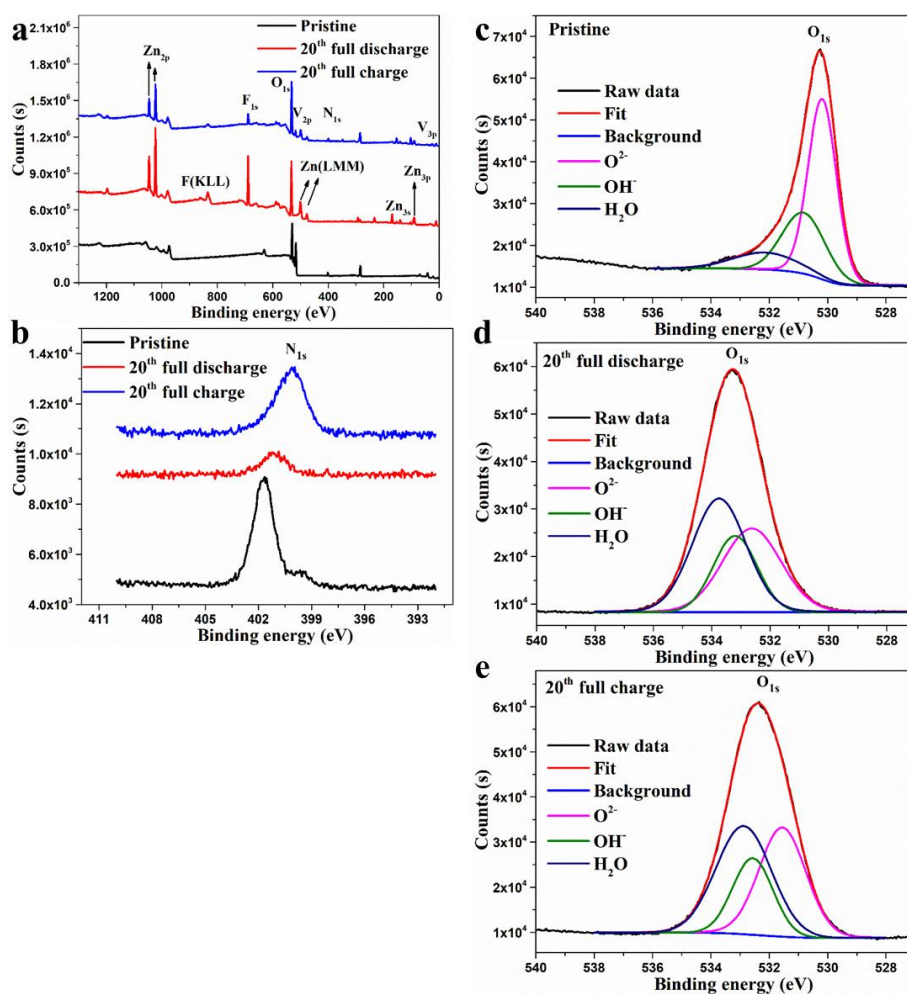


Figure S9. *Ex situ* full XPS spectra (a), N_{1s} core-level XPS spectra (b) and O_{1s} core-level XPS spectra (c-e) of the cathode materials at different discharge/charge states in Zn// $(\text{NH}_4)_2\text{V}_4\text{O}_9$ battery.

References

- (1) Alfuruqi, M. H.; Mathew, V.; Song, J.; Kim, S.; Islam, S.; Pham, D. T.; Jo, J.; Kim, S.; Baboo, J. P.; Xiu, Z. et al. Electrochemical Zinc Intercalation in Lithium Vanadium Oxide: A High-Capacity Zinc-Ion Battery Cathode. *Chem. Mater.* **2017**, *29*, 1684.
- (2) Peng, Z.; Wei, Q.; Tan, S.; He, P.; Luo, W.; An, Q.; Mai, L. Novel layered iron vanadate cathode for high-capacity aqueous rechargeable zinc batteries. *Chem. Commun.* **2018**, *54*, 4041.
- (3) Hu, P.; Yan, M.; Zhu, T.; Wang, X.; Wei, X.; Li, J.; Zhou, L.; Li, Z.; Chen, L.; Mai, L. Zn/V2O5 Aqueous Hybrid-Ion Battery with High Voltage Platform and Long Cycle Life. *ACS Appl. Mater. Interfaces* **2017**, *9*, 42717.
- (4) Jo, J. H.; Sun, Y.-K.; Myung, S.-T. Hollandite-type Al-doped VO_{1.52}(OH)_{0.77} as a zinc ion insertion host material. *J. Mater. Chem. A* **2017**, *5*, 8367.
- (5) He, P.; Quan, Y.; Xu, X.; Yan, M.; Yang, W.; An, Q.; He, L.; Mai, L. High-Performance Aqueous Zinc-Ion Battery Based on Layered H₂V₃O₈ Nanowire Cathode. *Small* **2017**, *13*, 1702551.
- (6) Yan, M.; He, P.; Chen, Y.; Wang, S.; Wei, Q.; Zhao, K.; Xu, X.; An, Q.; Shuang, Y.; Shao, Y. et al. Water-Lubricated Intercalation in V₂O₅·nH₂O for High-Capacity and High-Rate Aqueous Rechargeable Zinc Batteries. *Adv. Mater.* **2018**, *30*, 1703725.
- (7) Tang, B.; Fang, G.; Zhou, J.; Wang, L.; Lei, Y.; Wang, C.; Lin, T.; Tang, Y.; Liang, S. Potassium vanadates with stable structure and fast ion diffusion channel as cathode for rechargeable aqueous zinc-ion batteries. *Nano Energy* **2018**, *51*, 579.
- (8) Shan, L.; Yang, Y.; Zhang, W.; Chen, H.; Fang, G.; Zhou, J.; Liang, S. Observation of combination displacement/intercalation reaction in aqueous zinc-ion battery. *Energy Storage Mater.* **2019**, *18*, 10.
- (9) Fang, G.; Zhou, J.; Cai, Y.; Liu, S.; Tan, X.; Pan, A.; Liang, S. Metal-organic framework-templated two-dimensional hybrid bimetallic metal oxides with enhanced lithium/sodium storage capability. *Journal of Materials Chemistry A* **2017**, *5*, 13983.
- (10) Sambandam, B.; Soundharajan, V.; Kim, S.; Alfuruqi, M. H.; Jo, J.; Kim, S.; Mathew, V.; Sun, Y.-k.; Kim, J. Aqueous rechargeable Zn-ion batteries: an imperishable and high-energy Zn₂V₂O₇ nanowire cathode through intercalation regulation. *J. Mater. Chem. A* **2018**, *6*, 3850.
- (11) Xia, C.; Guo, J.; Lei, Y.; Liang, H.; Zhao, C.; Alshareef, H. N. Rechargeable Aqueous Zinc-Ion Battery Based on Porous Framework Zinc Pyrovanadate Intercalation Cathode. *Adv. Mater.* **2018**, *30*, 1705580.
- (12) Wu, X.; Xiang, Y.; Peng, Q.; Wu, X.; Li, Y.; Tang, F.; Song, R.; Liu, Z.; He, Z.; Wu, X. Green-low-cost rechargeable aqueous zinc-ion batteries using hollow porous spinel ZnMn₂O₄ as the cathode material. *Journal of Materials Chemistry A* **2017**, *5*, 17990.
- (13) Cai, Y.; Liu, F.; Luo, Z.; Fang, G.; Zhou, J.; Pan, A.; Liang, S. Pilotaxitic Na_{1.1}V₃O_{7.9} nanoribbons/graphene as high-performance sodium ion battery and aqueous zinc ion battery cathode. *Energy Storage Mater.* **2018**, *13*, 168.
- (14) Zhang, N.; Cheng, F.; Liu, J.; Wang, L.; Long, X.; Liu, X.; Li, F.; Chen, J. Rechargeable aqueous zinc-manganese dioxide batteries with high energy and power densities. *Nat Commun* **2017**, *8*, 405.
- (15) Islam, S.; Alfuruqi, M. H.; Mathew, V.; Song, J.; Kim, S.; Kim, S.; Jo, J.; Baboo, J. P.; Pham, D. T.; Putro, D. Y. et al. Facile synthesis and the exploration of the zinc storage mechanism of β-MnO₂ nanorods with exposed (101) planes as a novel cathode material for high performance eco-friendly zinc-ion batteries. *Journal of Materials Chemistry A* **2017**, *5*, 23299.

- (16) Jiang, B.; Xu, C.; Wu, C.; Dong, L.; Li, J.; Kang, F. Manganese Sesquioxide as Cathode Material for Multivalent Zinc Ion Battery with High Capacity and Long Cycle Life. *Electrochimica Acta* **2017**, *229*, 422.
- (17) Hao, J.; Mou, J.; Zhang, J.; Dong, L.; Liu, W.; Xu, C.; Kang, F. Electrochemically induced spinel-layered phase transition of Mn_3O_4 in high performance neutral aqueous rechargeable zinc battery. *Electrochimica Acta* **2018**, *259*, 170.
- (18) Lu, K.; Song, B.; Zhang, Y.; Ma, H.; Zhang, J. Encapsulation of zinc hexacyanoferrate nanocubes with manganese oxide nanosheets for high-performance rechargeable zinc ion batteries. *Journal of Materials Chemistry A* **2017**, *5*, 23628.
- (19) Li, W.; Wang, K.; Cheng, S.; Jiang, K. A long-life aqueous Zn-ion battery based on $\text{Na}_3\text{V}_2(\text{PO}_4)_2\text{F}_3$ cathode. *Energy Storage Mater.* **2018**, *15*, 14.
- (20) Tang, B.; Zhou, J.; Fang, G.; Liu, F.; Zhu, C.; Wang, C.; Pan, A.; Liang, S. Engineering the interplanar spacing of ammonium vanadates as a high-performance aqueous zinc-ion battery cathode. *J. Mater. Chem. A* **2019**, *7*, 940.
- (21) Wei, T.; Li, Q.; Yang, G.; Wang, C. Highly reversible and long-life cycling aqueous zinc-ion battery based on ultrathin $(\text{NH}_4)_2\text{V}_10\text{O}_{25}\cdot 8\text{H}_2\text{O}$ nanobelts. *Journal of Materials Chemistry A* **2018**, DOI:10.1039/C8TA06626D 10.1039/C8TA06626D.
- (22) Yang, G.; Wei, T.; Wang, C. Self-Healing Lamellar Structure Boosts Highly Stable Zinc-Storage Property of Bilayered Vanadium Oxides. *ACS Appl. Mater. Interfaces* **2018**, *10*, 35079.
- (23) Kundu, D.; Adams, B. D.; Duffort, V.; Vajargah, S. H.; Nazar, L. F. A high-capacity and long-life aqueous rechargeable zinc battery using a metal oxide intercalation cathode. *Nature Energy* **2016**, *1*, 16119.
- (24) Ming, F.; Liang, H.; Lei, Y.; Kandambeth, S.; Eddaoudi, M.; Alshareef, H. N. Layered $\text{Mg}_x\text{V}_2\text{O}_5\cdot n\text{H}_2\text{O}$ as Cathode Material for High-Performance Aqueous Zinc Ion Batteries. *ACS Energy Lett.* **2018**, *3*, 2602.
- (25) Xia, C.; Guo, J.; Li, P.; Zhang, X.; Alshareef, H. N. Highly Stable Aqueous Zinc-Ion Storage Using a Layered Calcium Vanadium Oxide Bronze Cathode. *Angew. Chem. Int. Ed.* **2018**, *57*, 3943.
- (26) He, P.; Zhang, G.; Liao, X.; Yan, M.; Xu, X.; An, Q.; Liu, J.; Mai, L. Sodium Ion Stabilized Vanadium Oxide Nanowire Cathode for High-Performance Zinc-Ion Batteries. *Adv. Energy Mater.* **2018**, *8*, 1702463.
- (27) Guo, X.; Fang, G.; Zhang, W.; Zhou, J.; Shan, L.; Wang, L.; Wang, C.; Lin, T.; Tang, Y.; Liang, S. Mechanistic Insights of Zn^{2+} Storage in Sodium Vanadates. *Adv. Energy Mater.* **2018**, *8*, 1801819.
- (28) Hu, P.; Zhu, T.; Wang, X.; Wei, X.; Yan, M.; Li, J.; Luo, W.; Yang, W.; Zhang, W.; Zhou, L. et al. Highly Durable $\text{Na}_2\text{V}_6\text{O}_{16}\cdot 1.63\text{H}_2\text{O}$ Nanowire Cathode for Aqueous Zinc-Ion Battery. *Nano Lett.* **2018**, *18*, 1758.
- (29) Chao, D.; Zhu, C.; Song, M.; Liang, P.; Zhang, X.; Tiep, N. H.; Zhao, H.; Wang, J.; Wang, R.; Zhang, H. et al. A High-Rate and Stable Quasi-Solid-State Zinc-Ion Battery with Novel 2D Layered Zinc Orthovanadate Array. *Adv. Mater.* **2018**, *30*, 1803181.
- (30) Ding, J.; Du, Z.; Gu, L.; Li, B.; Wang, L.; Wang, S.; Gong, Y.; Yang, S. Ultrafast Zn^{2+} Intercalation and Deintercalation in Vanadium Dioxide. *Adv. Mater.* **2018**, *30*, 1800762.
- (31) Park, J.-S.; Jo, J. H.; Aniskevich, Y.; Bakavets, A.; Ragoisha, G.; Streltsov, E.; Kim, J.; Myung, S.-T. Open-Structured Vanadium Dioxide as an Intercalation Host for Zn Ions: Investigation by First-Principles Calculation and Experiments. *Chem. Mater.* **2018**, *30*, 6777.
- (32) Wei, T.; Li, Q.; Yang, G.; Wang, C. An electrochemically induced bilayered structure facilitates long-life zinc storage of vanadium dioxide. *J. Mater. Chem. A* **2018**, *6*, 8006.

- (33) Dai, X.; Wan, F.; Zhang, L.; Cao, H.; Niu, Z. Freestanding graphene/VO₂ composite films for highly stable aqueous Zn-ion batteries with superior rate performance. *Energy Storage Mater.* **2019**, *17*, 143.
- (34) Pang, Q.; Sun, C.; Yu, Y.; Zhao, K.; Zhang, Z.; Voyles, P. M.; Chen, G.; Wei, Y.; Wang, X. H₂V₃O₈ Nanowire/Graphene Electrodes for Aqueous Rechargeable Zinc Ion Batteries with High Rate Capability and Large Capacity. *Adv. Energy Mater.* **2018**, *8*, 1800144.
- (35) Wei, T.; Li, Q.; Yang, G.; Wang, C. High-rate and durable aqueous zinc ion battery using dendritic V₁₀O₂₄·12H₂O cathode material with large interlamellar spacing. *Electrochim. Acta* **2018**, *287*, 60.
- (36) Zhang, N.; Dong, Y.; Jia, M.; Bian, X.; Wang, Y.; Qiu, M.; Xu, J.; Liu, Y.; Jiao, L.; Cheng, F. Rechargeable Aqueous Zn–V₂O₅ Battery with High Energy Density and Long Cycle Life. *ACS Energy Lett.* **2018**, *3*, 1366.
- (37) Chen, X.; Wang, L.; Li, H.; Cheng, F.; Chen, J. Porous V₂O₅ nanofibers as cathode materials for rechargeable aqueous zinc-ion batteries. *Journal of Energy Chemistry* **2019**, *38*, 20.
- (38) Lai, J.; Zhu, H.; Zhu, X.; Koritala, H.; Wang, Y. Interlayer-Expanded V₆O₁₃·nH₂O Architecture Constructed for an Advanced Rechargeable Aqueous Zinc-Ion Battery. *ACS Appl. Energy Mater.* **2019**, *2*, 1988.
- (39) Liu, F.; Chen, Z.; Fang, G.; Wang, Z.; Cai, Y.; Tang, B.; Zhou, J.; Liang, S. V₂O₅ Nanospheres with Mixed Vanadium Valences as High Electrochemically Active Aqueous Zinc-Ion Battery Cathode. *Nano-Micro Lett.* **2019**, *11*, 25.
- (40) Li, Y.; Huang, Z.; Kalambate, P. K.; Zhong, Y.; Huang, Z.; Xie, M.; Shen, Y.; Huang, Y. V₂O₅ nanopaper as a cathode material with high capacity and long cycle life for rechargeable aqueous zinc-ion battery. *Nano Energy* **2019**, *60*, 752.
- (41) Qin, H.; Chen, L.; Wang, L.; Chen, X.; Yang, Z. V₂O₅ hollow spheres as high rate and long life cathode for aqueous rechargeable zinc ion batteries. *Electrochim. Acta* **2019**, *306*, 307.
- (42) He, P.; Yan, M.; Zhang, G.; Sun, R.; Chen, L.; An, Q.; Mai, L. Layered VS₂ Nanosheet-Based Aqueous Zn Ion Battery Cathode. *Adv. Energy Mater.* **2017**, *7*, 1601920.
- (43) Qin, H.; Yang, Z.; Chen, L.; Chen, X.; Wang, L. A high-rate aqueous rechargeable zinc ion battery based on the VS₄@rGO nanocomposite. *J. Mater. Chem. A* **2018**, *6*, 23757.
- (44) Zhang, N.; Cheng, F.; Liu, Y.; Zhao, Q.; Lei, K.; Chen, C.; Liu, X.; Chen, J. Cation-Deficient Spinel ZnMn₂O₄ Cathode in Zn(CF₃SO₃)₂ Electrolyte for Rechargeable Aqueous Zn-Ion Battery. *J. Am. Chem. Soc.* **2016**, *138*, 12894.